Time-Domain Reduced-Order Models of Lateral Viscous Damping Effects for 3-D Geometries

Po-Ching Yen and Yao-Joe Yang
Department of Mechanical Engineering
National Taiwan University
1 Roosevelt Rd. Sec 4., Taipei, Taiwan, ROC
yjy@ccms.ntu.edu.tw, TEL:+886 2 23646491 FAX:+886 2 23631755

ABSTRACT

A methodology of generating time-domain reduced-order models of viscous lateral damping effects for microsystems is presented. A three-dimensional finite-difference-method (FDM) Stokes flow solver was developed and verified. The system matrices generated by the solver was then reduced to low-order macromodels, which can be easily inserted into a system-level modeling package for transient and frequency analysis. The simulated results of the FDM Stokes solver and the reduced-order macromodels are verified with the analytical solution. The reduced-order models have been to be about two-order-of-magnitude as efficient as the FDM solver. Transient simulations also indicate that friction stress of 3D models result in more damping effects than those estimated by the 1-D analytical models.

Keywords: Stokes' equation, lateral damping, model order reduction, macromodel, Stokes flow

INTRODUCTION

Devices with lateral motion are common in MEMS, especially for those devices built with comb-drive mechanisms. Modeling of lateral viscous damping of 3-D geometries requires meshing the air films surrounding the moving structures, and thus needs considerable computational resources. Therefore, previous works on lateral viscous damping for 3-D structures were based on 1-D analytical Stokes and Couette flow solutions [1-3]. Aluru [4] developed a 3-D Stokes flow solver using boundary-element-method (BEM). This work and the follow-up works [5,6] demonstrated that the BEM approaches not only require much less computational cost than typical FEM/FDM approaches, but also significantly reduce the efforts on creating solid models. However, since the solutions of BEM approaches are in frequency domain, each computation is for a specific frequency. Although there are some techniques for transforming frequency-response curves into time-domain models [7], the transformed time-domain models are not guaranteed to be stable [8]. In this work, we developed a time-domain 3-D FDM Stokes solver, and created time-domain reduced-order models using Arnoldi-based algorithm [9,10] from the original FDM models. In order to verify the results of the 3-D FDM solver, the simulated velocity profiles are compared with 1-D analytical solutions for the cases of sinusoidal oscillation and constant velocity. The procedure of generating reduced-order models is also described. The transient simulated viscous stress results of the reduced-order models are also verified with the analytical solutions.

VERIFICATION

A. 1-D Analytical Solutions

The governing equation of lateral viscous damping is the Stokes equation. The 3-D Stokes' equation is [11]:

$$\rho\frac{\partial\vec{V}}{\partial t} = -\nabla p + \mu\nabla^2\vec{V} \qquad (1)$$

where p is pressure, ρ is the density of the gas, μ is the viscosity coefficient, and $\vec{V} = [u \quad v \quad w]^t$ is the velocity vector. For our case, the imposed pressure gradient is assumed to be zero, so the first term on the right-hand side of Equation 1 is eliminated. Note that for typical thin-plate-type or comb-drive-type MEMS devices under in-plane motion, the damping force is dominated by the shearing stress. Also, since the damping contributed by the surfaces, whose normal vectors are parallel to the direction of plate motion, is negligible under our assumptions, the velocity components perpendicular to the direction of the in-plane motion are ignored, and the continuity equation is not considered.

Assume that an initially stationary fluid is set into unsteady motion by a lateral movement (x direction) of a solid surface which is infinite in x and y direction, as shown in Figure 1, the 3-D Stokes equation can be simplified to

$$\frac{\partial u}{\partial t} = \upsilon\frac{\partial^2 u}{\partial z^2} \qquad (2)$$

where u is velocity in x-direction, and $\upsilon = \mu/\rho$ is the kinetic viscosity

CASE I

For a moving surface oscillating in periodic motion, the boundary conditions are:

$$u(0,t) = \mathrm{Re}[u_0 e^{i\omega t}], \quad u(\infty,t) = 0 \tag{3}$$

and the solution [11,12] is:

$$u = u_0 \cos\left(\omega t - \sqrt{\frac{\omega}{2\upsilon}} z\right) e^{-\sqrt{\frac{\omega}{2\upsilon}} z} \tag{4}$$

The solution is in fact a strongly damped wave penetrating in z-direction, and the "penetration depth" is proportional to $\sqrt{\upsilon/\omega}$.

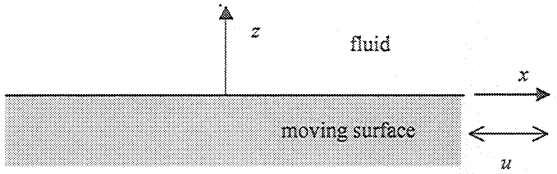

Figure 1 *Schematic of an initially stationary fluid driven by a moving surface.*

CASE II

For a surface initially at rest then acquiring a constant velocity u_0 at $t=0$, the boundary conditions are:

$$u(0,t) = u_0, \quad u(\infty,t) = 0$$

and the solution is:

$$\begin{aligned} u &= u_0 \frac{2}{\sqrt{\pi}} \int_{z/2\sqrt{\upsilon t}}^{\infty} e^{-\eta^2} d\eta \\ &\equiv u_0 \left[1 - erf\left(\frac{z}{2\sqrt{\upsilon t}}\right)\right] \end{aligned} \tag{5}$$

The solutions for both cases give velocity profiles as functions of z. The penetration depth is proportional to $\sqrt{\upsilon t}$. Due to the assumption of infinite-sized surfaces, the solutions neglect the velocity variation in x and y directions, and thus the solutions do not include the edge effects for finite-sized moving plates. In order to estimate the edge effects more precisely, a 3-D FDM Stokes' solver is developed.

B. Comparison of 1-D Analytical Solutions with the Results of 3-D FDM Stokes Solver

A simulated example for the 3-D FDM Stokes solver is shown in Figure 2. The computational domain is the space between the outer box and the inner plate. The plate is moving or oscillating in x-direction. The 3-D governing equation approximated by FDM is:

$$\rho \frac{\partial u}{\partial t} = \mu\left(\frac{\partial^2 u}{\partial x^2} + \frac{\partial^2 u}{\partial y^2} + \frac{\partial^2 u}{\partial z^2}\right) \tag{6}$$

The gas properties used in our simulation are listed in Table 1. The plate size is 600 μmx400 μmx20 μm. Both the cases of oscillating moving-boundary (CASE I) and the constant-velocity moving boundary (CASE II) are considered. The comparisons are made between the analytical solutions and the calculated velocity profiles extended from *the center of the plate surface.* Note that because the 3-D FDM solver accounts for the edge effect due to finite plate size, the edge effect is minimized on the center of the plate surface.

Viscosity coefficient	Gas density	Kinetic viscosity
μ=18.5x10^{-6} Ns/m^2	ρ=1.1766 kg/m^3	ν=15.73x10^{-6} m^2/s

Table 1 *Gas properties used in this work.*

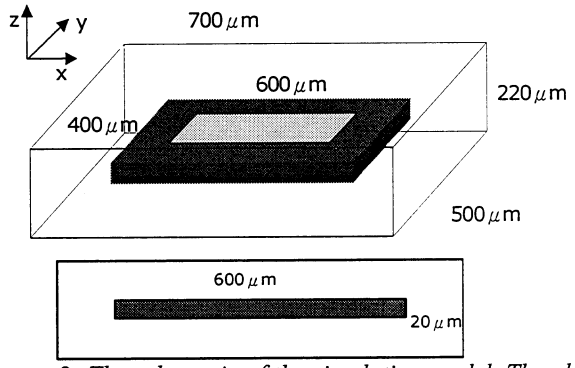

Figure 2 *The schematic of the simulation model. The plate is 600 μmx400 μmx20 μm. The light-shaded region on the top of the plate is "the central part of the plate".*

Figure 3 shows the velocity profiles of FDM results and analytical solution for oscillating moving boundary condition (CASE I). The curves shown in the figure are the velocity profiles for π /6 intervals in a half oscillation period after the whole system reaches sinusoidal steady-state. The velocity decays as the fluid is away from the oscillation surface. The simulated results are in good agreement with the analytical solution. Note that for this case, the oscillation frequency is 10kHz.

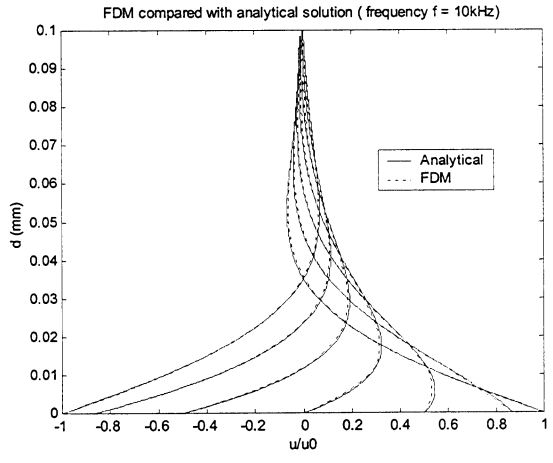

Figure 3 *Velocity profiles of the analytical solution and FDM solver in the ambient pressure (above the central part of the oscillating plate) with oscillating moving boundary. Profiles are shown for π/6 intervals over half a period.*

The comparison of simulated results and analytical solutions for CASE II is shown in Figure 4. The curves in the figure are the velocity profiles for different time steps. The velocity profile expands further into the fluid as the time increases.

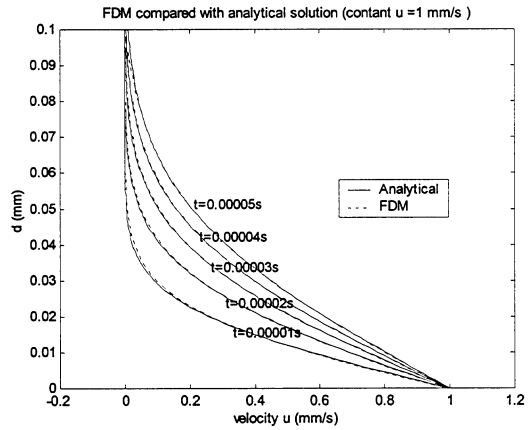

Figure 4 *Velocity profiles of the analytical solution and FDM solver (above the central part of the plate) with constant velocity. Profiles are shown from $1x10^{-5}$ to $5x10^{-5}$ sec with 10^{-5} sec interval.*

THEORY OF MODEL ORDER REDUCTION

Although the 3-D FDM Stokes solver give us accurate transient results for different moving boundary conditions, as described in the previous section, the computational cost is very expensive due to the significant large number of nodes in the 3-D fluidic computational domain. Fortunately, the governing equation, as shown in Equation 6, is a linear equation, and the system matrices generated by FDM approximation process for Equation 6 can be reduced by an Arnoldi-based model order reduction (MOR) technique. The dynamic system equation generated by the FDM approximation of Equation 6 is

$$\begin{aligned} \dot{x} &= Ax + Bu \\ y &= C^T x + Du \end{aligned} \tag{7}$$

where A is an n by n matrix and n is the total number of nodes, x is the vector which contains the unknown velocity distribution on each node, and the input function, u, is the imposed velocity on the moving boundary of the computational domain. In this case, we carefully formulate C and D, so that the output y will be the frictional shear (calculated by Newtonian law of viscosity) on the plate. In Laplace domain, the transfer function of the system is:

$$\begin{aligned} T(s) &= C^T(Is - A)^{-1}B + D = C^T(I - sA^{-1})^{-1}b + D \\ b &= -A^{-1}B \end{aligned} \tag{8}$$

After expanding the transfer function in Taylor series about s=0, we obtain:

$$T(s) = C^T(I + sA^{-1} + s^2A^{-2} + \ldots)b = \sum_{k=0}^{\infty} m_k s^k \tag{9}$$

where m_k are the coefficients of the Taylor series, ($m_k = C^T(A^{-k})b$). The Taylor expansion can be truncated to approximate the transfer function $T(s)$. Since $A^{-k}b$ quickly line up with a single eigenvector, this moment matching procedure is usually numerically unstable. Therefore, we apply the Arnoldi-based algorithm to stably compute orthogonal bases v_i that spans the Krylov subspace:

$$K_q(A^{-1}, b) = span\{b, A^{-1}b, A^{-2}b, \cdots, A^{-(q-1)}b\} \tag{10}$$

Given the matrix V whose columns are $\{v_i\}$, the reduced order model is

$$\begin{aligned} \dot{x}_q &= A_q x_q + B_q u \\ y &= C_q^T x_q + Du \end{aligned} \tag{11}$$

where

$$A_q = v^T A v \quad B_q = v^T B$$
$$C_q = v^T C$$

Note that the reduced system, as shown in Equation 11, has the same input (u) and output (y) as Equation 7. Since the typical sizes of A_q, B_q and C_q are very small, the computational efficiency for simulating transient responses and frequency responses of the reduced models are significantly increased.

RESULTS

A. FDM results

The FDM simulated domain (as shown in Figure 1) was meshed into 83283 nodes. The steady-state velocity profiles for a plate moving in a constant velocity are shown in Figure 5. Figures 5-(a) and -(b) indicate that the profile near the edge of the plate has larger velocity gradient than that at the central part of the plate.

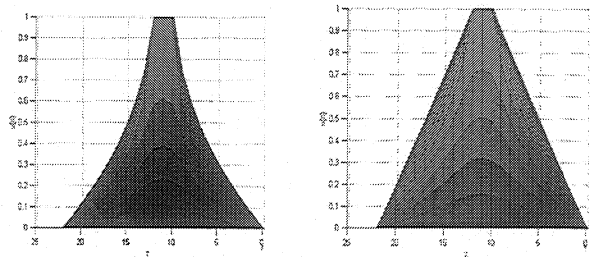

Figure 5 *The velocity distributions of the plate moving in x direction. Figure (a) shows the velocity profiles close to the plate edges. Figure (b) shows the results on the central part.*

B. MOR Results and Comparison between MOR and FDM

The main purpose of MOR techniques is to reduce the

order of the system so that the computational performance will be improved with limited compromise in accuracy. The results of the macromodels generated by MOR technique are compared with results by the 3-D FDM solver. The preliminary numerical experiments show that the results from a reduced model of order 20 match with FDM results very well.

Figure 6 shows that when the plate moves with constant velocity u = 1 mm/s, the total shear stress surrounding the plate will decrease from 1.5×10^{-2} N/mm^2 to a steady state value of 2×10^{-3} N/mm^2 at about 3×10^{-4} sec. It also shows that the 20th-order curve of the macromodel is in good agreement with the FDM result.

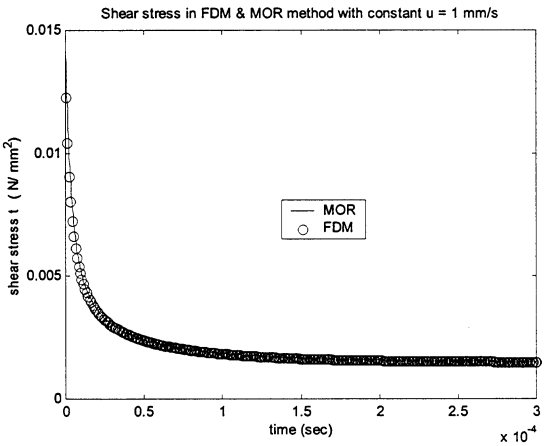

Figure 6 *Shear stress τ calculated by a macromodel and the FDM solver, for the plate moving in constant velocity.*

If the plate oscillated in a periodic motion, we find the amplitude of the shear stress is less then that in the plate with constant velocity. However, as the oscillating frequency increases, the amplitude also increases. Figure 7 shows that the shear stress curves in FDM and 20th-order MOR, and indicates that the curves match very well.

The comparison on computational times is listed on Table 2. About 100-times or better improvement on computational performance has been demonstrated.

	Constant Velocity	Sinusoidal Oscillation
FDM	195 sec	194 sec
MOR	2 sec	0.5 sec

Table 2 *Comparison of computational times between FDM and MOR*

CONCLUSION

This paper presented a 3-D FDM Stokes' solver, and a macromodel generation methodology for lateral damping effects based on the application of Arnoldi-based model-reduction technique. The results by the 3-D FDM solver were carefully verified with analytical solutions. The theory of the Arnoldi-based model-order-reduction is described. Macromodels of order 20 generated by the MOR techniques are simulated, and their results agree with the results by the 3-D FDM solver. The comparison of total computation times for different cases was also provided. An average decrease in computational time by two orders of magnitude was demonstrated.

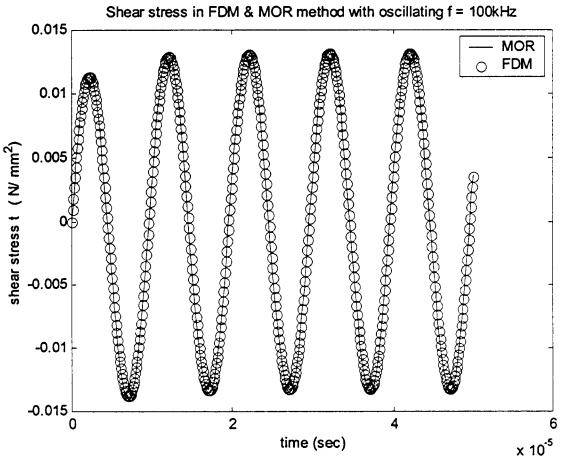

Figure 7 *Shear stress τ calculated by a macromodel and the FDM solver, for the plate oscillating in periodic motion.*

REFERENCES

1. Y.-H. Cho, et. al., "Viscous Damping Model for Laterally Oscillating Microstructures," J. MEMS, vol. 3, no. 2, June 1994, pp. 81-87.
2. X. Zhang, et. al., "Viscous Air Damping in laterally driven microresonator," Sensors and Materials, vol. 7, no. 6, pp. 415-430, 1995.
3. T. Veijola, "Compact Damping Models for Lateral Structures Including Gas Rarefaction Effects,"
4. N. R. Aluru, et. al., "A fast integral equation technique for analysis of microflow sensors based on drag force calculations," Proc. Of MSM, 283-286, 1998.
5. W. Ye, et. al., "Viscous Drag on A Lateral Micro-Resonator: Fast 3-D Fluid Simulation and Measured Data", Tech. Digest, Solid-State Sensor and Actuator Workshop, Hilton Head Island, SC, June 2000, pp 124-127.
6. X. Wang, et. al., "Analyzing Fluid Compression Effects in Complicated Micro-machined Devices," Trans. 2001, pp. 666-669.
7. C. Coelho, et. al., "Robust Rational Function Approx. Algorithm for Model Generation," DAC 99, 1999.
8. Personal communication with Dr. M. Kamon and Dr. V. Rabinovich.
9. Y.-J. Yang, et. al. "Modeling Gas Damping and Spring Phenomena In MEMS With Frequency Dependent Macro-Models" IEEE MEMS 2001.
10. A. Odabasioglu, el. al., "PRIMA," IEEE Transaction on Computer-Aided Design of Integrated Circuits and Systems, Vol. 17, No. 8, August 1998.
11. J. A. Fay, Introduction to Fluid Mechanics, MIT Press, Cambridge, 1994.
12. F. K. Moore, Theory of Laminar Flow, Princeton University Press, Princeton, 1964.